Surface Hydride Composition of Plasma-Synthesized Si Nanoparticles

ARTICLE *in* THE JOURNAL OF PHYSICAL CHEMISTRY C · SEPTEMBER 2011

Impact Factor: 4.77 · DOI: 10.1021/jp2028005

THE JOURNAL OF PHYSICAL CHEMISTRY C

ARTICLE

pubs.acs.org/JPCC

Surface Hydride Composition of Plasma-Synthesized Si Nanoparticles

Bhavin N. Jariwala,[†] Nicolaas J. Kramer,[‡] M. Cristina Petcu,[‡] David C. Bobela,[§] M. C. M. van de Sanden,[‡] Paul Stradins,[§] Cristian V. Ciobanu,[*,∥] and Sumit Agarwal[*,†]

[†]Department of Chemical Engineering, Colorado School of Mines, Golden, Colorado 80401, United States

[‡]Department of Applied Physics, Eindhoven University of Technology, 5600 MB Eindhoven, The Netherlands

[§]National Center for Photovoltaics, National Renewable Energy Laboratory, Golden, Colorado 80401, United States

[∥]Department of Mechanical Engineering, Colorado School of Mines, Golden, Colorado 80401, United States

Supporting Information

ABSTRACT: We have determined the surface hydride composition of amorphous and crystalline Si nanoparticles (NPs) (3−5 nm) synthesized in a low-temperature SiH_4/Ar plasma using in situ attenuated total reflection Fourier-transform infrared spectroscopy and H_2 thermal effusion measurements. With increasing power to the plasma source, the particles transition from amorphous to crystalline with a corresponding increase in the fraction of SiH species on the surface. The surface hydride composition indicates that Si NPs synthesized at higher plasma powers crystallize in the gas-phase due to a greater degree of plasma-induced heating, which enhances the desorption rates for SiH_2 and SiH_3. Furthermore, these Si NPs do not contain any detectable H in the bulk.

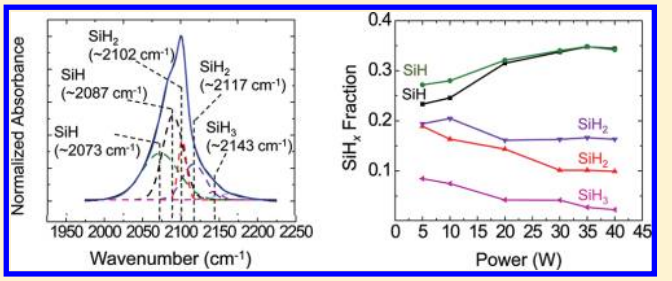

Reducing the size of crystalline Si (*c*-Si) nanoparticles (NPs) below 5 nm gives rise to new properties compared to bulk silicon due to quantum confinement effects. Quantum-confined Si NPs exhibit a tunable, size-dependent band gap, visible photoluminescence (PL), and multiple-exciton generation.[1−3] Quantum confinement effects have also been demonstrated in amorphous Si NPs embedded in a dielectric matrix.[4−6] Furthermore, it has been shown that the optical properties of Si NPs not only depend on their size and structure (crystalline vs amorphous) but also on the surface functionalization[1] and surface oxidation.[7]

Several plasma synthesis techniques have been used to grow quantum-confined Si NPs.[8−11] Among these techniques, a continuous-flow, nonthermal, radio frequency (rf) plasma produces freestanding NPs over a size range of 3−10 nm with a size distribution of ±10%.[8] Synthesis of NPs in a SiH_4 plasma inherently leads to H-terminated surfaces due to the abundance of atomic H in the discharge.[12] Although surface hydrides provide some degree of defect passivation, such H-terminated Si NPs are not chemically stable in atmosphere and oxidize rapidly.[13] At the same time, the H-terminated surface of Si NPs provides an opportunity to functionalize their surface using different ligands to prevent oxidation and to further passivate any dangling bonds defects present on the surface.[12,13] The surface of *c*-Si NPs can however be quite complex due to the different facets and reconstructions that result in different types of surface hydride species (SiH_x, x = 1,2,3) with different reactivity to a surface passivating agent.[12] It is therefore essential to obtain a systematic understanding of the surface structure and composition of plasma-synthesized Si NPs to develop strategies for surface functionalization. Here, we report the surface composition of *c*-Si and amorphous Si (*a*-Si) NPs synthesized in a nonthermal SiH_4/Ar rf plasma, determined using in situ attenuated total reflection Fourier-transform infrared (ATR-FTIR) spectroscopy.

Si NPs were synthesized in a low-temperature, capacitively coupled plasma generated in a quartz tube with an inner diameter of 7.5 mm with an rf power input at 13.56 MHz ranging from 5 to 40 W. SiH_4 (1.4 sccm), heavily diluted in Ar (275 sccm), was introduced into the quartz tube with the discharge generated between two Cu ring electrodes placed around the tube. The powered electrode was closer to the upstream end of the tube at a distance of 5 cm from the stainless steel quick-coupling flange. The grounded electrode was placed 3 cm further in the downstream direction. During gas flow, the upstream pressure was 4.3 Torr while the base pressure was <1 mTorr. The above flow rates, electrode arrangement, and pressure were essential for powder formation in our reactor: other configurations resulted in *a*-Si particles irrespective of the rf power or excessive film deposition on the walls of the quartz tube. The downstream end of the quartz tube was attached to a stainless steel vacuum chamber equipped with an in situ ATR-FTIR spectroscopy setup

Received: March 25, 2011
Revised: August 23, 2011
Published: September 07, 2011

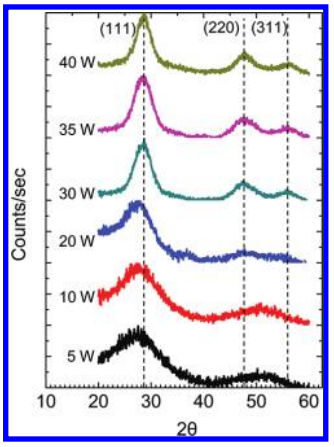

Figure 1. X-ray diffraction spectra for the NPs synthesized at various plasma powers. Peaks corresponding to the (111), (220), and (311) crystallographic planes become visible as the plasma power increases.

described in detail previously.[14] The Si NPs exiting the quartz tube were collected on a ZnSe internal reflection element (IRE), which was in line of sight with the gas exiting from the quartz tube. A spectral resolution of 4 cm^{-1} was employed during the collection of all the infrared (IR) spectra. The NPs were also collected on a Si wafer placed near the IRE for ex situ characterization using X-ray diffraction (XRD) (Siemens Kristalloflex 810, Cu Kα source), transmission electron microscopy (TEM) (Philips CM200 with Princeton Gamma-Tech Prism Energy Dispersive X-ray Spectrometer) and PL spectroscopy. Prior to ex situ characterization, the Si NPs were exposed to the atmosphere, which results in surface oxidation. Therefore, during ex situ characterization, the Si NPs were in a slightly differently physical state than the particles characterized in situ with IR spectroscopy.

Thermal desorption of H_2 was measured using a quartz effusion tube prepared by baking an empty tube under vacuum, $\sim 10^{-6}$ Torr, at 800 °C. This ensured a clean tube, with little background contamination from adsorbed H_2O etc. The tube was then sealed under vacuum, $\sim 10^{-6}$ Torr, and brought to a glovebox where the Si NPs, collected on a stainless steel mesh, were transferred into the tube. The tube was backfilled with N_2 and brought back to the effusion station where it was evacuated to low pressures. Thus, the Si NPs were not exposed to the ambient, and the effusion studies should provide a direct comparison with the in situ IR data. The sample effusion tube was placed into a cylindrical, temperature-controlled oven at room temperature and the quadrupole mass spectrometer (QMS) attached to the vacuum system was turned on. The sample was pumped down to a pressure of $\sim 5 \times 10^{-7}$ Torr, which ensured very low baseline signals. The temperature was then ramped at 10 °C/min and the H_2^+ signal was collected using the QMS. Ambient H_2O, O_2, CO_2, and N_2 signals were also monitored during the measurement to confirm that there was minimal sample contamination during the transfer process.

The XRD patterns for as-synthesized Si NPs at various plasma powers are shown in Figure 1. The XRD patterns for NPs synthesized at lower powers were similar to those previously observed for plasma-deposited amorphous hydrogenated Si (*a*-Si:H).[15] At higher plasma powers ($\geq$35 W), well-defined peaks corresponding to the (111), (220), and (311) lattice planes of Si are observed in Figure 1, indicating that the NPs were crystalline.

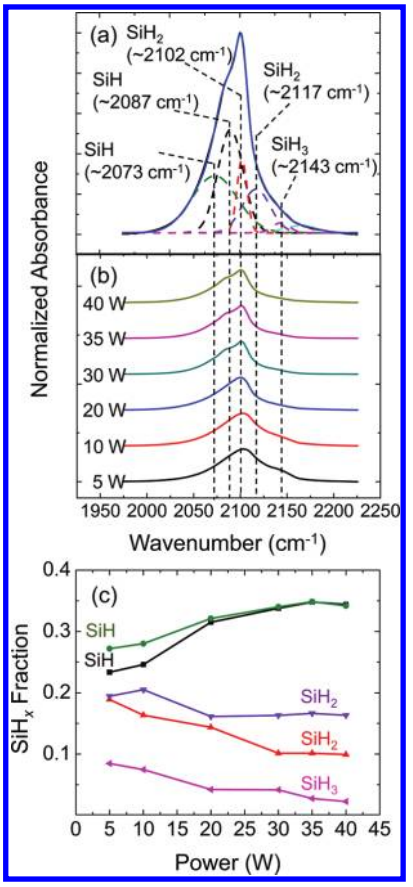

Figure 2. (a) Deconvoluted SiH_x (x = 1,2,3) stretching region showing the various stretching modes for NPs synthesized at 40 W. The cumulative fit is shown in blue, and the original data is shown in black. (b) IR spectra showing the SiH_x (x = 1,2,3) stretching region for NPs synthesized at various powers. (c) Fractional integrated absorbance for the different stretching modes plotted as a function of the plasma power. The color of the plots in (c) corresponds to the color of the deconvoluted stretching modes in (a). All the IR spectra are normalized.

This is also consistent with previous work by Mangolini and coworkers, who reported an increase in Si NP crystallinity due to higher particle temperatures in the plasma at higher rf powers. Mangolini et al. associated the particle heating with highly exothermic ion-electron and neutral-neutral radical recombination reactions occurring on the NP surface.[8] By use of Raman spectroscopy, Anthony and Kortshagen further confirmed that the broadening of the XRD peaks at lower plasma powers was due to a decrease in NP crystallinity.[16] Our XRD peaks for the *c*-Si NPs are still relatively broad compared to bulk *c*-Si.[17] This peak broadening compared to bulk *c*-Si is most likely due to the particle size distribution combined with the strain at the surface of the nanocrystals. TEM micrographs indicate that the Si NPs are over the size range of 3−5 nm (see TEM image in Figure S1 of the Supporting Information).

The change in surface composition with increasing crystallinity of the Si NPs was determined by measuring their composition using in situ ATR-FTIR spectroscopy. The IR spectra of the NPs clearly show that their surface is H-terminated (Figure 2). Figure 2a shows the deconvolution of the SiH_x (x = 1,2,3) stretching region for NPs synthesized at 40 W. The SiH_x (x = 1,2,3) stretching region between 2000 and 2200 cm^{-1} consists of several stretching vibrations, which result from Si mono-, di-,

and trihydrides on the surface and in the bulk film.[18] Since Si NPs with diameters below 5 nm are spherical in shape and do not contain large and well-defined facets,[19,20] the surface has a large number of small terraces with numerous edges and atomic steps. Thus, SiH, SiH_2, and SiH_3 observed on the NP surface are similar to those observed on a mixture of small H-terminated crystallographic planes with a substantial number of steps and edges. The spectra in Figure 2 were deconvoluted with five Gaussian line shapes using peak assignments available in the literature for both *c*-Si and *a*-Si surfaces.[18,21,22] Since the ranges of peak positions of different surface hydrides on *a*-Si and *c*-Si overlap,[18,21] the hydride stretching region was fitted using almost identical peak positions (± 2 cm^{-1}) for *a*-Si and *c*-Si NPs with only slight variations in the peak widths (± 6 cm^{-1}) (please refer to Figure S2 and Tables S3 and S4 of Supporting Information). Specifically, we assigned the bands at ~2073 and ~2090 cm^{-1} to surface SiH, ~2102 and ~2117 cm^{-1} to surface SiH_2, and the single peak at ~2143 cm^{-1} to surface SiH_3 stretching modes.[18,21,22] Moreover, the peak positions corresponding to SiH, SiH_2, and SiH_3 on various crystallographic orientations overlap,[23] and the Gaussians employed in this work can be further deconvoluted to include such additional peaks. However, since the surface of <5 nm *c*-Si NPs in not fully known (as it consists of many small facets/terraces and edges with undetermined orientations and sizes), we have limited the number of peaks to the minimum required to fit the IR data accurately. A small peak for SiH back-bonded to oxygen (<2% of the total integrated absorbance) was also included to incorporate the effect of oxidation. However, the near absence of the Si−O−Si antisymmetric stretching transverse optic phonon band at ~1050 cm^{-1} indicates that oxidation is insignificant under vacuum. The surface hydride stretching modes occur at a higher frequency than the corresponding vibrations in the bulk film.[18] Additionally, the fwhm of the surface modes is generally 30−40 cm^{-1} smaller than that of bulk hydride modes.[18] Thus, based on the position and fwhm of each Gaussian, we have concluded that the different stretching modes observed in our experiments correspond only to surface SiH_x (x = 1,2,3) species.[18,21,22] In particular, the absence of the bulk SiH stretching vibration at 2000 cm^{-1}, which is a signature absorption band for *a*-Si:H,[18] indicates that the plasma-synthesized *a*-Si NPs are very different than plasma-deposited a-Si:H despite the similarity of their XRD patterns. The structure rather corresponds to H-terminated tetrahedral Si with different bond lengths and bond angles than those in perfect *c*-Si. Moreover, the absence of peaks below 2000 cm^{-1} for both *c*-Si and *a*-Si NPs suggests that the NPs do not contain mono- or divacancy defects which are responsible for hydride stretching modes below 2010 cm^{-1}.[24]

Figure 2b shows the SiH_x (x = 1,2,3) stretching region for NPs synthesized at different plasma powers. A clear difference in the SiH_x (x = 1,2,3) stretching region can be observed between NPs synthesized at 40 and 5 W, corresponding to *c*-Si and *a*-Si NPs, respectively. As the plasma power (or the crystallinity of the NPs) increases, the shoulder associated with the SiH_3 stretch mode at ~2143 cm^{-1} subsides and a prominent shoulder at ~2088 cm^{-1} corresponding to the SiH stretching mode emerges. The surface hydride composition of the NPs at various powers was further compared by normalizing the integrated absorbance of the different stretching modes to the total integrated absorbance of the SiH_x band and plotting these fractions as a function of the plasma power (see Figure 2c). We have observed that as the plasma power increases the fractions for the

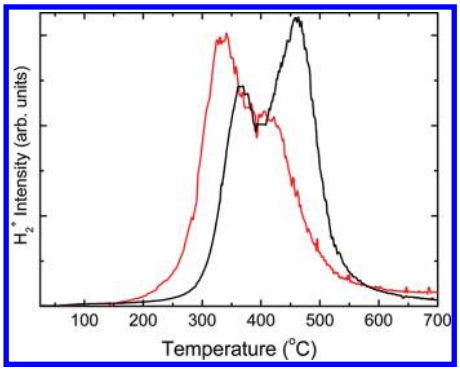

Figure 3. H_2 desorption from amorphous (red) and crystalline (black) Si NPs as a function of temperature.

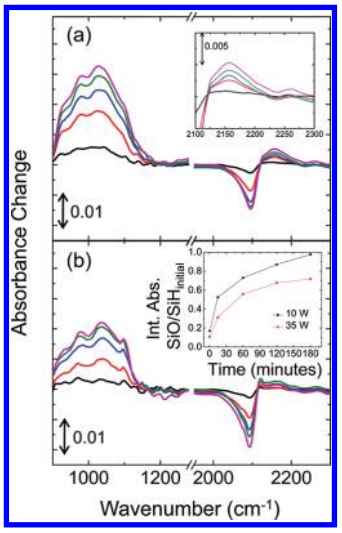

Figure 4. IR difference spectra showing controlled oxidation of NPs synthesized at (a) 10 W and (b) 35 W at various time intervals. The inset in (a) is a magnification of the 2100−2300 cm^{-1} region of the IR spectrum in (a) to illustrate the absorbance increase due to a shift in SiH_x (x = 1,2) stretching vibrations due to backbonding of surface Si with O atoms. The inset in (b) shows the plot of the normalized integrated area absorbance of the SiO_x stretch (centered at ~1050 cm^{-1}) for NPs synthesized at 10 and 35 W as a function of the oxidation time. The integrated area of the SiO_x stretching region is normalized with the corresponding integrated area of the SiH_x stretching region of as-synthesized NPs at 10 and 35 W.

SiH_2 and SiH_3 stretching modes decrease while the SiH fraction increases; in other words, the SiH fraction increases with an increase in crystallinity. To understand particle crystallization, Mangolini and co-workers proposed a theoretical model based on experimentally measured ion and atomic H densities in a SiH_4/Ar plasma.[25] The model demonstrated that although Si NPs undergo several temperature fluctuations (hundreds of Kelvins above room temperature) during growth, the surface of these NPs is at all times almost entirely H-terminated due to abundance of atomic H in a SiH_4/Ar plasma.[25] Thus, we can conclude that the surface hydride composition depends on the temperature of these NPs during their growth in the gas-phase. Furthermore, it is well-known in the literature that as the temperature of reconstructed H-terminated Si(100)[26,27] and Si(111),[27,28] and porous Si[29] surfaces increases, SiH_2 and SiH_3 thermally desorb at lower temperatures than SiH. A similar

dx.doi.org/10.1021/jp2028005 |*J. Phys. Chem. C* 2011, 115, 20375–20379

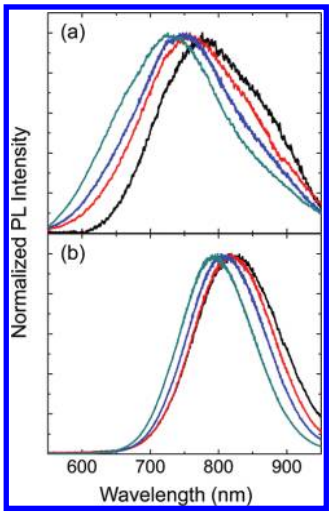

Figure 5. Normalized PL spectra of NPs synthesized at (a) 10 W and (b) 35 W and exposed to atmosphere. The curves (right to left) represent the PL spectra after 1, 2, 4, and 6 days of exposure to atmosphere.

trend has also been previously demonstrated for Si quantum dots using temperature-programmed desorption measurements.[30]

Our H_2 thermal effusion measurements for Si NPs synthesized at 10 and 35 W rf power validate the in situ IR measurements and show that the Si NPs synthesized at low plasma powers have a higher fraction of lower hydrides (see Figure 3). The two primary peaks observed in both H_2 effusion spectra in Figure 3 correspond to the β_1 (high temperature, 400−450 °C) and β_2 (low temperature, 300−350 °C) peaks for effusion from mono- and dihydrides, respectively. These observations are consistent with the IR spectra that show that the fraction of dihydrides is higher for *a*-Si NPs compared to *c*-Si NPs. This is also consistent with the absence of hydrides in the bulk of the Si NPs. In amorphous and microcrystalline Si films that contain a void structure where the SiH frequency may resemble the surface modes observed in the IR spectra in Figure 2, the low-temperature effusion peak generally appears at 100 °C, which is absent in our spectra.[31] The lower SiH_2 and SiH_3 fractions observed in our experiments for NPs synthesized at higher powers therefore suggests that these NPs were formed at higher temperatures, at which the less stable SiH_2 and SiH_3 desorbed from the surface preferentially.

To study the oxidation of the H-terminated Si NPs, a controlled set of experiments were performed by exposing the particles to O_2 (99.999%) at 30 mTorr pressure in the vacuum chamber. In each experiment, an IR difference spectrum, which represents changes on the surface of the NPs due to interaction with O_2, was collected every 5 min to observe the oxidation process. These IR spectra are shown in Figure 4. Three distinct peaks corresponding to oxidized NPs were observed at ∼1050, ∼2160, and ∼2250 cm^{-1}. The broad band at ∼1050 cm^{-1} corresponds to the different SiO_x phonon modes and the remaining two peaks correspond to SiH_x (x = 1,2) stretching modes where the Si atom is back-bonded to one or more O atoms.[32] The oxidation of the NPs was also accompanied by an overall decrease in absorbance due to the SiH_x (x = 1,2,3) stretching modes (see Figure 4). To compare the rate of oxidation of *a*-Si and *c*-Si NPs, the integrated absorbance change for the SiO_x stretching region was normalized with the integrated absorbance change for the SiH_x stretching region in the as-synthesized NPs: this was necessary since the particle yield varied with different plasma powers. The temporal evolution of the normalized integrated absorbance change for SiO_x phonons in the inset of Figure 4b shows that the *a*-Si NPs synthesized at 10 W oxidized faster than c-Si NPs synthesized at 35 W. Moreover, PL measurements using 514.5 nm excitation from an Ar^+ laser and a Si CCD detector were performed at room temperature on as-synthesized NPs collected on a Si wafer. PL measurements were made after 1, 2, 4, and 6 days. Special precaution was exercised to ensure that the laser fluence did not result in localized heating of the NPs, which could lead to an increase in the oxidation rate. Furthermore, in each case, the PL intensity was measured at 3−4 different spots on the sample using a low laser power of ∼7 mW, and the spectra were averaged for 5 s. Figure 5 shows the normalized room-temperature PL spectra at various time intervals for NPs synthesized at 10 and 35 W. The PL spectra for both *a*-Si and *c*-Si NPs shift to higher energies due to oxidation. The PL shift for the crystalline NPs can be explained by shrinking of the Si core of the NP because of oxidation.[33] Since the crystalline NPs (3−6 nm) are quantum-confined, the decrease in size of the crystalline core leads to an increase in the band gap and a corresponding blue-shift in the PL peak.[33] However, the PL observed from the *a*-Si sample could arise from the *a*-Si NPs themselves or from a small fraction of *c*-Si NPs that may also be present. If the PL was indeed due to a small fraction of *c*-Si NPs in the amorphous sample, and if the *c*-Si NPs were approximately the same size as the NPs in the crystalline samples, then the rate of oxidation and, hence, the shift in PL should be similar. But from Figure 5 it can be clearly seen that the blue shift in the PL for the amorphous sample is faster than the shift in the crystalline sample. This strongly suggests that the PL originates from the *a*-Si NPs and not from a small fraction of *c*-Si NPs in the amorphous sample. This is consistent with quantum confinement effects previously demonstrated in *a*-Si NPs embedded in a dielectric.[4] While our data suggest that the observed blue-shift in PL is due to quantum confinement effects, it should be noted that PL from Si NPs has also been related to surface defects.[7]

In summary, we have determined the surface SiH_x (x = 1,2,3) composition of plasma-synthesized NPs ranging from amorphous to crystalline. On the basis of the in situ ATR-FTIR spectroscopy measurements we conclude that the *c*-Si NPs have a higher fraction of SiH on the surface as compared to amorphous NPs. Our measurements thus imply that *c*-Si NPs synthesized at higher plasma powers crystallize in the gas-phase due to a greater degree of plasma-induced heating, which enhances the desorption rates for SiH_2 and SiH_3 compared to SiH. Further, an interesting inference from the IR measurements is that the plasma-synthesized *c*-Si and *a*-Si NPs do not contain any detectable H in the bulk, and thus, no vacancy defects where these H atoms would be bonded. This shows that the plasma-synthesized *a*-Si NPs are clearly distinct from *a*-Si:H. In situ IR and PL measurements show that *a*-Si NPs oxidize faster than *c*-Si NPs.

■ ASSOCIATED CONTENT

Supporting Information. Tables depicting peak assignments (positions and widths) employed to fit IR spectra for *c*-Si NPs synthesized at high plasma powers (30, 35, and 40 W) and peak assignments (positions and widths) employed to fit IR spectra for *a*-Si NPs synthesized at low plasma powers (5, 10, and 20 W). Figures depicting the transmission electron image of nanocrystals synthesized at 40 W and normalized IR spectra showing the deconvoluted SiHx (x = 1,2,3) stretching region for

nanoparticles synthesized at 5−35 W. This material is available free of charge via the Internet at http://pubs.acs.org.

AUTHOR INFORMATION

Corresponding Author
*E-mail: sagarwal@mines.edu (S.A.); cciobanu@mines.edu (C.V.C.).

ACKNOWLEDGMENT

This research was supported by NSF (Grant Nos. CMMI-0846858 and CBET-0846923), the CRSP program (Task No. KXFE-9-99001-08), the Renewable Energy MRSEC program at the Colorado School of Mines (NSF Grant No. DMR-0820518), the Eindhoven University of Technology, and the U.S. DOE Solar Energy Technology Program (Contract No. DE-AC36-08GO28308). We thank Dr. Reuben T. Collins for support with photoluminescence measurements, and Mr. Gary Zito for assistance with the TEM work.

REFERENCES

(1) Jurbergs, D.; Rogojina, E.; Mangolini, L.; Kortshagen, U. *Appl. Phys. Lett.* **2006**, *88*, 233116.
(2) Reboredo, F. A.; Franceschetti, A.; Zunger, A. *Phys. Rev. B* **2000**, *61*, 13073.
(3) Beard, M. C.; Knutsen, K. P.; Yu, P. R.; Luther, J. M.; Song, Q.; Metzger, W. K.; Ellingson, R. J.; Nozik, A. J. *Nano Lett.* **2007**, *7*, 2506.
(4) Park, N. M.; Choi, C. J.; Seong, T. Y.; Park, S. J. *Phys. Rev. Lett.* **2001**, *86*, 1355.
(5) Wang, Y. Q.; Chen, W. D.; Liao, X. B.; Cao, Z. X. *Nanotechnology* **2003**, *14*, 1235.
(6) Pi, X. D.; Zalloum, O. H. Y.; Roschuk, T.; Wojcik, J.; Knights, A. P.; Mascher, P.; Simpson, P. J. *Appl. Phys. Lett.* **2006**, *88*, 103111.
(7) Wolkin, M. V.; Jorne, J.; Fauchet, P. M.; Allan, G.; Delerue, C. *Phys. Rev. Lett.* **1999**, *82*, 197.
(8) Mangolini, L.; Thimsen, E.; Kortshagen, U. *Nano Lett.* **2005**, *5*, 655.
(9) Batson, P. E.; Heath, J. R. *Phys. Rev. Lett.* **1993**, *71*, 911.
(10) Li, X. G.; He, Y. Q.; Talukdar, S. S.; Swihart, M. T. *Langmuir* **2003**, *19*, 8490.
(11) Onischuk, A. A.; Levykin, A. I.; Strunin, V. P.; Ushakova, M. A.; Samoilova, R. I.; Sabelfeld, K. K.; Panfilov, V. N. *J. Aerosol Sci.* **2000**, *31*, 879.
(12) Mangolini, L.; Kortshagen, U. *Adv. Mater.* **2007**, *19*, 2513.
(13) Gupta, A.; Wiggers, H. *Physica E* **2009**, *41*, 1010.
(14) Jariwala, B. N.; Ciobanu, C. V.; Agarwal, S. *J. Appl. Phys.* **2009**, *106*, 073305.
(15) Ray, P. P.; Gupta, N. D.; Chaudhuri, P.; Williamson, D. L.; Vignoli, S.; Longeaud, C. *J. Non-Cryst. Solids* **2002**, *299*, 123.
(16) Anthony, R.; Kortshagen, U. *Phys. Rev. B* **2009**, *80*, 115407.
(17) Martin-Palma, R. J.; Pascual, L.; Herrero, P.; Martinez-Duart, J. M. *Appl. Phys. Lett.* **2005**, *87*, 211906.
(18) Agarwal, S.; Takano, A.; van de Sanden, M. C. M.; Maroudas, D; Aydil, E. S. *J. Chem. Phys.* **2002**, *117*, 10805.
(19) Hadjisavvas, G.; Remediakis, I. N.; Kelires, P. C. *Phys. Rev. B* **2006**, *74*, 165419.
(20) Wang, Y. Q.; Smirani, R.; Ross, G. G. *Nano Lett.* **2004**, *4*, 2041.
(21) Chabal, Y. J.; Higashi, G. S.; Raghavachari, K.; Burrows, V. A. *J. Vac. Sci. Technol. A* **1989**, *7*, 2104.
(22) Niwano, M.; Terashi, M.; Kuge, J. *Surf. Sci.* **1999**, *420*, 6.
(23) Kolasinski, K. W.; Hartline, J. D.; Kelly, B. T.; Yadlovskiy, J. *Mol. Phys.* **2010**, *108*, 1033.
(24) Smets, A. H. M.; van de Sanden, M. C. M. *Phys. Rev. B* **2007**, *76*, 073202.
(25) Mangolini, L.; Kortshagen, U. *Phys. Rev. E* **2009**, *79*, 026405.
(26) Cheng, C. C.; Yates, J. T. *Phys. Rev. B* **1991**, *43*, 4041.
(27) Greenlief, C. M.; Gates, S. M.; Holbert, P. A. *J. Vac. Sci. Technol. A* **1989**, *7*, 1845.
(28) Greenlief, C. M.; Gates, S. M.; Holbert, P. A. *Chem. Phys. Lett.* **1989**, *159*, 202.
(29) Zoubir, N. H.; Vergnat, M. *Appl. Surf. Sci.* **1995**, *89*, 35.
(30) Salivati, N.; Ekerdt, J. G. *Surf. Sci.* **2009**, *603*, 1121.
(31) Beyer, W. *Sol. Energy Mater. Sol. Cells* **2003**, *78*, 235.
(32) Mawhinney, D. B.; Glass, J. A.; Yates, J. T. *J. Phys. Chem. B* **1997**, *101*, 1202.
(33) Ledoux, G.; Guillois, O.; Porterat, D.; Reynaud, C.; Huisken, F.; Kohn, B.; Paillard, V. *Phys. Rev. B* **2000**, *62*, 15942.